PRP Pharmacology Research & Perspectives
Open Access

ORIGINAL ARTICLE

The cardioprotective efficacy of TVP1022 against ischemia/reperfusion injury and cardiac remodeling in rats

Assaf Malka[1], Offir Ertracht[2], Noa Bachner-Hinenzon[3], Irina Reiter[4] & Ofer Binah[4,]

[1]Faculty of Medicine in the Galilee, Bar-Ilan University, Safed, Israel
[2]Eliachar Research Laboratory, Galilee Medical Center, Nahariya, Israel
[3]Migal Galilee Technology Center, Department of Computational Science and Bioinformatics, Kiryat Shmona, Israel
[4]Department of Physiology, Biophysics and Systems Biology, the Rappaport Faculty of Medicine and Research Institute, Technion, Haifa, Israel

Keywords
Cardioprotection, ischemia/reperfusion, myocardial infarction, remodeling, TVP1022

Correspondence
Ofer Binah, Department of Physiology, Biophysics and Systems Biology. Ruth & Bruce Rappaport Faculty of Medicine, Technion – Israel Institute of Technology, PO Box 9649, Haifa 31096, Israel. Tel: +972 4 8295262; Fax: +972 4 8513919; E-mail: binah@tx.technion.ac.il

Funding Information
This work was supported by the Alfred Mann Institute at the Technion.

Received: 10 July 2016; Revised: 20 September 2016; Accepted: 27 September 2016

Pharma Res Per, 4(6), 2016, e00272, doi:10.1002/prp2.272

doi: 10.1002/prp2.272

Abstract

Following acute myocardial infarction (MI), early and successful reperfusion is the most effective strategy for reducing infarct size and improving the clinical outcome. However, immediate restoration of blood flow to the ischemic zone results in myocardial damage, defined as "reperfusion-injury". Whereas we previously reported that TVP1022 (the S-isomer of rasagiline, FDA-approved anti-Parkinson drug) decreased infarct size 24 h post ischemia reperfusion (I/R) in rats, in this study we investigated the chronic cardioprotective efficacy of TVP1022 14 days post-I/R. To simulate the clinical settings of acute MI followed by reperfusion therapy, we employed a rat model of left anterior descending artery occlusion for 30 min followed by reperfusion and a follow-up for 14 days. TVP1022 was initially administered postocclusion–prereperfusion, followed by chronic daily administrations. Cardiac performance and remodeling were evaluated using customary and advanced echocardiographic methods, hemodynamic measurements by Millar Mikro-Tip® catheter, and histopathological techniques. TVP1022 administration markedly decreased the remodeling process as illustrated by attenuation of left ventricular enlargement and cardiac hypertrophy (both at the whole heart and the cellular level). Furthermore, TVP1022 inhibited cardiac fibrosis and reduced ventricular BNP levels. Functionally, TVP1022 treatment preserved cardiac wall motion. Specifically, the echocardiographic and most of the direct hemodynamic measures were pronouncedly improved by TVP1022. Collectively, these findings indicate that TVP1022 provides prominent cardioprotection against I/R injury and post-MI remodeling in this I/R model.

Abbreviations

AP, apical/apex; BNP, brain natriuretic peptide; BW, body weight; CHF, chronic heart failure; CO, cardiac output; CS, circumferential strain; CVF, collagen volume fraction; EDA, end diastolic area; EDP, end diastolic pressure; EDV, end diastolic volume; EF, Ejection fraction; ESA, end systolic area; ESP, end systolic pressure; ESV, end systolic volume; FS, fractional shortening; HR, heart rate; HW, heart weight; I/R, ischemia/reperfusion; LAD, left anterior descending; LV, left ventricle; MI, myocardial infarction; *N*-propargyl-1-(*S*)-aminoindan, TVP1022; NRVM, neonatal rat ventricular myocytes; PBS, phosphate-buffered saline; PCI, percutaneous coronary intervention; PM, papillary muscle; P-V, pressure-volume; STE, speckle tracking echocardiography; SV, stroke volume; SW, stroke work.

Introduction

Following acute myocardial infarction (MI), early and successful reperfusion by thrombolytic therapy or primary percutaneous coronary intervention (PCI) are most effective strategies for reducing infarct size and improving clinical outcome (Yellon and Hausenloy 2007; Antman et al. 2008). However, immediate restoration of blood flow to the ischemic zone can result in myocardial damage, termed "reperfusion injury" (Black 2000). This injury is attributed mainly to the oxygen-derived free radicals generated during the reperfusion, initiating an apoptotic cell death at the infarct and at its adjacent zones (Spinale 2010). The main efforts for myocardial salvage is focused on minimizing infarct size by technical measures such as PCI, although there is a favorable therapeutic window for interrupting the apoptotic process (days and weeks after injury), thus achieving long-term benefits (Dorn 2009).

TVP1022 is the S-isomer of rasagiline (Azilect) (FDA-approved anti-Parkinson's drug) (Fig. S1). Although TVP1022 is 1000 times less potent monoamine oxisdase B inhibitor than rasagiline, both isomers feature similar cytoprotective and neuroprotective efficacies (Huang et al. 1999; Youdim et al. 2005). Studies on the structure-activity relationship of TVP1022 showed that the neuroprotective effect is associated directly with its propargylamine moiety, and is ascribed to direct stabilization of mitochondrial membrane potential, induction of Bcl-2 and activation of PKC signaling pathway (Youdim et al. 2005). In agreement with its cytoprotective efficacy, TVP1022 was found to exert cardioprotective activities against doxorubicin and serum deprivation-induced apoptosis in neonatal rat ventricular myocytes (NRVM) (Kleiner et al. 2008; Berdichevski et al. 2010), and against ischemia/reperfusion (I/R) and chronic heart failure (CHF) in in vivo rat models (Abassi et al. 2011; Ertracht et al. 2011). In a thorough in vitro study, we investigated the mechanism underlying TVP1022 cardioprotection against H_2O_2-induced cell death in rat H9c2 cardiomyoblasts and NRVM (Ertracht et al. 2011). Briefly, TVP1022 dose-dependently inhibited H_2O_2-induced cytotoxicity, loss of mitochondrial membrane potential (Ψm) and release of mitochondrial cytochrome *c*. Furthermore, we discovered the involvement of the PKC and GSK-3β pathways in the cardioprotective effect of TVP1022 (Ertracht et al. 2011).

On the basis of these findings, we hypothesized that TVP1022 will provide cardioprotection against I/R injury and post-MI left ventricle (LV) remodeling in rats. Accordingly, we investigated the cardioprotective effects (14 days post-I/R) of TVP1022 administered intravenously (IV) only once 4 h post-MI, verses IV plus daily oral administration until sacrifice at day 14. Thus, our experimental model mimics the clinical scenario of MI treated with a cardioprotective drug prior to and following reperfusion therapy (IV at the hospital), with follow up period and chronic administrations (PO at home). In agreement with its previously reported cardioprotective efficacy, we found that TVP1022 treatment attenuated the remodeling process and preserved cardiac function. These results indicate that TVP1022 should be considered as a novel drug for treating MI injury and cardiac remodeling.

Materials and Methods

Animals

Experiments were conducted in male Sprague–Dawley rats (~8 weeks old, 280–320 g) (Harlan Laboratories, Ltd., Jerusalem, Israel) according to the institutional animal ethical committee guidelines which conform to the Guide for the Care and Use of Laboratory Animals published by the US National Institutes of Health (NIH Publication No. 85–23, revised 2011). Rats were maintained at the experimental surgical unit of the Technion Faculty of Medicine with a 12:12–h light-dark cycle and fed on normal rodent chow diet with tap water ad libitum, according to the Technion guidelines for animal care. All operators were blinded to treatment assignment.

Study design and the I/R experimental model

After baseline echocardiography scan (see details below), all animals underwent I/R surgery (see details below) followed by 14 days follow-up. On the last day of the protocol (day 14), rats underwent final echocardiography scan and direct cardiac function evaluation using Millar Mikro-Tip® catheter (see below). Finally, the rats were killed and their hearts harvested for off-line analyses.

Treatment groups and drug administration routes

The study consisted of five treatment groups: (1) MI + Vehicle; (2) MI + chronic TVP1022 (20 mg/kg); (3) MI + chronic TVP1022 (40 mg/kg); (4) MI + acute TVP1022 (IV-only) 40 mg/kg; (5) Sham-operated animals. TVP1022 administration was as follows: Groups 1, 2, and 3 were administered IV with a vehicle (group 1) or TVP1022 (groups 2, 3) 5 min before reperfusion, followed by a second dose PO 4 h post reperfusion, and then daily PO administrations until sacrifice (additional 13 experimental days) (Table 1). To distinguish between acute (on the infarct size) and chronic (on the remodeling process) beneficial effects of TVP1022, Group 4 was

Table 1. Experimental groups.

#	Group	I/R	TVP1022 5 min pre reperfusion	TVP1022 4 hrs post reperfusion	Long-term treatment (13 days)
1	MI + vehicle	Yes	Vehicle IV	Vehicle PO	Vehicle PO
2	MI + Chronic TVP1022 (20 mg/kg)	Yes	TVP1022 IV (20 mg/kg)	TVP1022 PO (20 mg/kg)	TVP1022 PO (20 mg/kg)
3	MI + Chronic TVP1022 (40 mg/kg)	Yes	TVP1022 IV (40 mg/kg)	TVP1022 PO (40 mg/kg)	TVP1022 PO (40 mg/kg)
4	MI + acute TVP1022 (40 mg/kg)	Yes	TVP1022 IV (40 mg/kg)	TVP1022 IV (40 mg/kg)	No
5	Sham	No	No	No	No

administered IV with TVP1022 5 minutes before reperfusion, followed by a second dose IV 4 h post reperfusion, without additional chronic administrations. Group 5 (the sham-operated rats) did not receive any treatment. For the IV route TVP1022 was dissolved in 0.5 mL normal saline (0.9%) to desired dosage (20 or 40 mg/kg) and heated to 37°C. The tail was cleaned with 70% ethanol and an intravenous cannulation (20 G) was performed. The drug solution and an additional 0.2 mL of saline were administered through the cannula at a rate of 1 mL/min. Vehicle animals were treated with the same volume of saline. For the IV-only group (group 4) the procedure was similar except that the tail vein cannula was removed only after the second IV administration 4 hours post reperfusion. For the PO route TVP1022 was dissolved in 0.5 mL double distilled water (DDW) to the desired dosage (20 or 40 mg/kg). The drug solution was administered daily through gavage to the treated rats. Vehicle animals were treated with the same volume of DDW.

Echocardiographic measurements

To perform echocardiographic scans the animals were lightly sedated with a mixture of ketamine (29 mg/kg) and xylazine (4.3 mg/kg). After sedation rats were placed in a left lateral decubitus position and scanned via a commercially available echo scanner Vivid^{TM} *i* ultrasound cardiovascular system (GE Healthcare Inc. Israel) using a 10S phased array pediatric transducer and a cardiac application with high temporal and spatial resolution. The transmission frequency was set to 10 MHz, at depth of 2.5 cm and a frame rate of 315 frames/second. Echocardiography cines were obtained according to the American Society of Echocardiography guidelines (Arias et al. 2013). Measurements included two parasternal short-axis sections at the papillary muscle (PM) and at the apical (AP) levels. Using EchoPAC Dimension 08 (GE Healthcare Inc., Norway) program, LV end diastolic area (EDA) and LV end systolic area (ESA) were measured. Ejection fraction (EF) and fractional shortening (FS) were calculated using M-Mode images. Ultrasound cines were also postprocessed by speckle tracking echocardiography (STE) program (EchoPAC Dimension 08, GE Healthcare Inc.) which tracks the movement of the myocardium and assesses LV circumferential strain (CS) (% from end diastolic state to end systolic state) (Rappaport et al. 2006; Popović et al. 2007). STE was found to correctly assess wall motion in the rat (Popović et al. 2007). Furthermore, CS is considered a sensitive measurement since it can be measured at both PM and AP levels using multiple points on the cardiac wall circumference (Rappaport et al. 2006).

I/R surgery

The I/R model was generated by LAD occlusion for 30 min as previously described (Bhindi et al. 2006). Briefly, rats were anesthetized with a combination of 87 mg/kg ketamine and 13 mg/kg xylazine (IM), intubated and mechanically ventilated at a rate of 80–90 cycles/min with a tidal volume of 1–2 mL/100 g. Subsequently, using a left thoracotomy the chest was opened, the pericardial sac dissected and the heart exposed. A single stitch was placed through the myocardium at a depth slightly greater than the perceived level of the LAD while taking care not to puncture the ventricular chamber. The suture was tightened by a loop that allowed its rapid opening. Five minutes prereperfusion TVP1022 or vehicle was administered IV. 30 min after the occlusion the suture was rapidly released in order to resume blood flow through the LAD. The chest was closed and the animals were allowed to recover. Overall 127 rats underwent the procedure; with a death rate of ~44% (85% did not recover from surgery, 10% died within 24 h of surgery as a result of an acute response to I/R and 5% died 3 days post I/R) a total of 71 rats survived the 2 weeks follow-up period.

Measurements of cardiac hemodynamics

For direct cardiac function evaluation, hemodynamic measurements were obtained by the Millar pressure-

volume (P-V) system (MPVS-300, Millar Instruments, Houston, TX, USA). The Millar P-V System simultaneously and continuously measures LV pressure and volume from the intact beating heart, producing characteristic P-V loops readings of which a variety of cardiovascular parameters, such as heart rate (HR), cardiac output (CO), stroke volume (SV), ejection fraction (EF), stroke work (SW), dP/dt_{max}, and dP/dt_{min} are derived. Following the last echocardiographic measurement, rats were placed on controlled heating pads and injected IP with inactin (sodium thiobutabarbital, 100 mg/kg) in order to deepen their anesthesia. Next, the rats were tracheotomized and intubated (0.5 cm long 50 PE tube) to facilitate breathing. The right carotid was exposed and ligated distally, the artery was clamped and incised, and a 0.5 cm long 90 PE tube was inserted as a catheter guide. A 2-Fr Mikro-Tip® catheter (SPR-838, Millar Instruments, Houston, TX, USA) was advanced through the guide into the LV under pressure control; a ligature was then tightened around the catheter to avoid blood loss (Pacher et al. 2008). After stabilization for 5 min, signals were continuously sampled at a sampling rate of 1000 samples/sec by the MPVS-300 system, recorded, and displayed on a personal computer by the PowerLab System and Chart5 software (AD Instruments, Colorado Springs, CO, USA) for 15–20 min. At the end of each experiment, 100 μL of hypertonic (30%) saline were injected intravenously, and from the shift of P-V relations, parallel conductance volume (Vp) was calculated by the software and used for the correction of the cardiac mass volume. Thereafter, the catheter was withdrawn and the animal killed.

Animal euthanasia and organ harvesting

Following the hemodynamic measurements, the chest cavity was opened, the heart harvested and weighed. The heart was dissected transversely at the PM level and preserved in 4% paraformaldehyde for paraffin embedding section or by cryofixation in liquid nitrogen for immunofluorescence staining. Paraffin-embedded blocks were cut by microtome into 5 μm slices and stained by Masson's trichrome.

Histopathology

For fibrosis evaluation collagen volume fraction (CVF) was calculated from the Masson's trichrome-stained slides as follows: four fields of view were digitally photographed from each slide (taken from the remote noninfarcted area) at ×400 magnifications, yielding a total of 16 fields (4 slides × 4 fields in each). Positive connective tissue staining was identified using the ImageJ software (NIH, Boston, USA http://rsb.info.nih.gov/ij) (connective tissue is stained bright blue). CVF was calculated as the mean ratio of connective tissue to the total tissue area (field of view) of all the measurements (Jalil et al. 1989).

Immuno-histopathology

Frozen tissue samples were mounted on Leica microtome and cryosections 5-μm thick were prepared. Cryosections were air-dried and fixed for 10 min in acetone (−20°C). After washing three times with phosphate-buffered saline (PBS), sections were incubated with 10% donkey serum for one hour to block nonspecific binding sites. Next, the samples were incubated overnight at 4°C with primary antibodies against dystrophin (1:75) (Sigma, St. Louis, MO, USA) and B-type natriuretic peptide (BNP) (1:500) (Abcam, Cambridge, MA, USA). After washing three times with PBS the samples were incubated with Alexa555 (1:100) or GFP (1:100) second antibodies for 1 h at room temperature. Nuclei were stained blue with 4′,6-diamidino-2-phenylindole (DAPI) (1:1000), rinsed with PBS and mounted with cover glasses using IMMUMOUNT (Thermo scientific, Waltham, MA, USA) mounting medium. The slides were visualized using inverted motorized fluorescent microscope (Axio observer Z1, Carl Zeiss, Oberkochen, Germany), with Colibri led illumination light source (Carl Zeiss).

Cryosections from the AP level in each case were used. All samples were immuno-labeled simultaneously with identical conditions of fixation and dilutions of primary and secondary antibodies. No fluorescence was detected in the absence of the primary antibody. For each heart at least 10 random fields of vision were analyzed (from the scar border and the remote zone) with a motorized fluorescent microscope (Axio observer Z1, Carl Zeiss) using ×40 and ×20 objective lenses (Carl Zeiss). Digital images were obtained by the Axiovision image acquisition and processing software (Axiovision 4.9, Carl Zeiss) using a CCD camera (Orca R2, Hamamatsu Photonics K.K., Japan). All images were obtained under the same conditions and acquisition protocols and were studied using Axiovision and ImageJ softwares. Myocyte area and diameter were determined from at least 50 myocytes per section by delineating the dystrophin-labeled myocytes (Abassi et al. 2011). Quantification of BNP was performed by measuring the fluorescence intensity using a range of 0–255 gray values. Arbitrary units of the fluorescence intensity were calculated per unit myocardial area ($AU/\mu m^2$) in three random fields of view (×400).

Statistical analysis

All results are presented as mean ± SEM. To compare between treatment groups of each protocol, one-way

analysis of variance (ANOVA) was used. To compare between parameters at different time points, two-way ANOVA was used. The Holm–Sidak test was used as the post hoc test whenever a significant difference was found by the ANOVA. $P < 0.05$ was considered statistically significant. The analysis was performed by the SigmaStat for windows version 3.11 (Systat Software Inc., San Jose, CA, USA).

Results

In this study, we tested the hypothesis that TVP1022 will attenuate LV remodeling after I/R insult in rats. Cardiac performance and left ventricular remodeling were evaluated using customary and advanced echocardiographic methods, hemodynamic measurements by Millar Mikro-Tip® catheter and histopathological techniques.

Physical measurements

Mean body weight (BW), heart weight (HW), and HW to BW (HW/BW) ratio are presented in Table 2. For evaluating post-MI hypertrophy, we measured HW and calculated HW/BW ratio for each rat. In agreement with the expected remodeling process, in the MI vehicle-treated rats HW and HW/BW ratio markedly increased compared to sham rats ($P < 0.05$). HW and HW/BW ratio of the TVP1022-treated rats were lower than in vehicle-treated rats ($P < 0.05$, Table 2), indicating that TVP1022 prevented post-MI hypertrophy.

Echocardiography

LV dimensions and cardiac function were determined by means of 2D echocardiographic measurements at the AP and PM levels. Figure 1 depicts representative B-mode short-axis cines of rats from the sham, vehicle, and TVP1022 treatment groups and the summary of the 2D measurements. In agreement with the expected post-MI remodeling process, 14 days post-MI, LVEDA, and LVESA were increased in all MI rats, both at the AP and PM levels ($P < 0.05$ vs. sham) (Fig. 1A–E). TVP1022 attenuated the post-MI LV enlargement. At the apex, which is the most affected section of the heart in this model, the increase in LVEDA was markedly attenuated in TVP1022-treated rats compared the vehicle-treatment ($P < 0.05$) (Fig. 1B). The LVESA increase was attenuated in the MI+TVP1022 (20 and 40 mg/kg) groups, but not in the "IV only" group (Fig. 1C). At the PM level LVEDA increase was mitigated only for the TVP1022 (40 mg/kg) group ($P < 0.05$ vs. MI+Vehicle, Fig. 1D) but not in the MI+TVP1022 (20 mg/kg) or (IV-only) groups, whereas LVESA increase was mitigated in all TVP1022-treated rats ($P < 0.05$ vs. MI+Vehicle, Fig. 1E). In summary, TVP1022 treatment attenuated the remodeling process represented by the LV dimensional measurements, demonstrating the cardioprotective efficacy of TVP1022. Moreover, TVP1022 affected the remodeling process in a dose–response manner.

Functionally, as depicted by the representative echocardiographic M-mode cines (Fig. 2A), the ventricular wall motion, EF, and FS were markedly reduced 14 days post-MI, with improvement in the TVP1022-treated rats. Specifically, in the vehicle-treated group EF and FS were reduced by 26% and 17%, respectively ($P < 0.05$ vs. baseline and vs. sham). Similar reductions were observed in the MI+TVP1022, "IV-only" group. In the MI+TVP1022 20 mg/kg and 40 mg/kg groups this reduction was attenuated ($P < 0.05$ vs. vehicle). Moreover, in the 20 mg/kg

Table 2. Physical measurements presented at the different treatment groups.

Time/Treatment	Baseline BW (g)	14 days BW (g)	14 days HW (g)	14 days HW/BW (mg/g)
MI + Vehicle ($n = 22$)	310 ± 4.8	322 ± 6.2	#1.25 ± 0.02	#3.92 ± 0.01
MI + TVP1022 (20 mg/kg) ($n = 14$)	311 ± 5.6	321 ± 9.7	*1.16 ± 0.06	*3.52 ± 0.03
MI + TVP1022 (40 mg/kg) ($n = 19$)	306 ± 4.1	322 ± 4.2	*1.09 ± 0.02	*3.35 ± 0.007
MI + TVP1022 IV-only ($n = 8$) (40 mg/kg)	321 ± 6.3	345 ± 5.9	*1.12 ± 0.03	*3.22 ± 0.005
Sham ($n = 8$)	314 ± 8.2	326 ± 9.6	1.09 ± 0.03	3.2 ± 0.007

BW, Body weight; HW, heart weight.
*$P < 0.05$ versus MI + Vehicle.
#$P < 0.05$ versus sham.

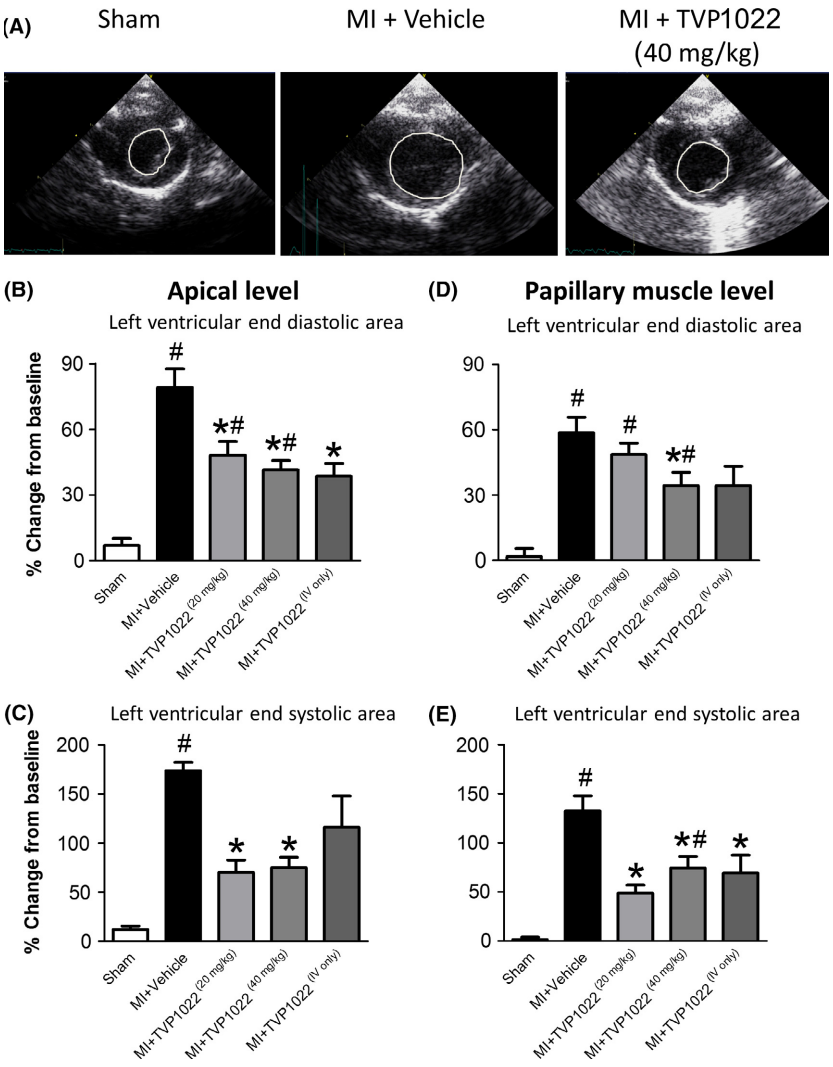

Figure 1. TVP1022 attenuated the enlargement in LV dimensions 14 days post-MI. (A) Representative apical level echocardiographic two-dimensional (2D) mode end-diastolic cines of the sham, MI+Vehicle and TVP1022 (40 mg/kg) groups (additional groups are depicted in Fig. S2A), white tracing – LV cavity; Echocardiographic 2D measurements obtained at the apical (B and C) and PM (D and E) levels. Left ventricular EDA (B and D) and ESA (C and E) [% change from baseline] measured in the different groups: MI+Vehicle (n = 22), MI+TVP1022 (20 mg/kg) (n = 14), MI+TVP1022, (40 mg/kg) (n = 19), MI+TVP1022 (IV-only) (n = 8) and sham (n = 8). *P < 0.05 versus MI+Vehicle, #P < 0.05 versus sham.

TVP1022-treated group, EF and FS were comparable to baseline ($P > 0.05$ vs. baseline, Fig 2B). Collectively, these results indicate that chronic (but not acute) TVP1022 treatment preserved ventricular function. A total of six rats were excluded from the M-MODE analysis (1 animal from the vehicle group, 3 from the TVP1022 20 mg/kg group and 2 from the TVP1022 40 mg/kg group) by the analyzer (the analyzer was blinded to the treatment groups) due to low quality of the obtained cine loops.

To obtain more sensitive and accurate assessments of LV function we measured global circumferential strain (CS) which represents ventricular contraction. Figure 3A depicts representative CS distribution along the cardiac wall, measured at the AP level 14 days post-MI, taken from sham operated, MI+Vehicle, and MI+TVP1022 (20 mg/kg) groups. The figure depicts B-mode cines where a colored CS map is superimposed on each cine; dark red colors represent strong CS and lighter red colors represent moderate CS; light blue colors represent mild stretching and dark blue represents severe stretching. As shown in Figure 3A the sham group is characterized by strong red colors (strong contraction), whereas in the vehicle-treated MI rats the red colors were markedly disrupted, turning light red and even blue. In contrast, in the TVP1022-treated rats global CS was preserved as illustrated by the reddish color of the CS map, lacking any

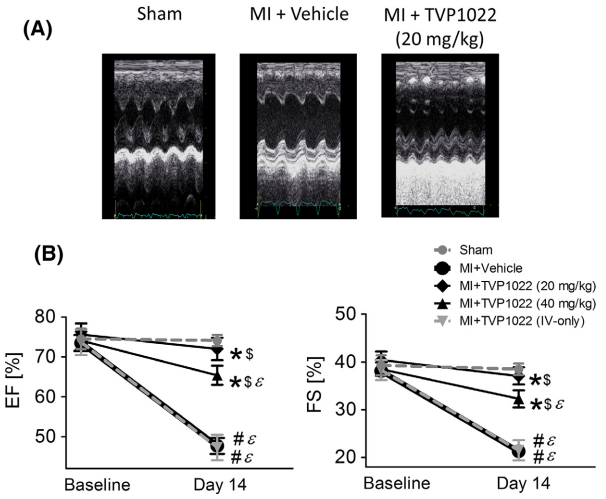

Figure 2. TVP1022 attenuated the decline in LV function 14 days post-MI. (A) representative echocardiographic M-mode cines obtained at the PM level for the sham, MI+Vehicle and TVP1022 (20 mg/kg) groups (additional groups are depicted in Fig. S2B). (B) EF and FS measured 14 days post-MI in the different groups: MI+Vehicle (n = 21), MI+TVP1022 (20 mg/kg) (n = 11), MI+TVP1022, (40 mg/kg) (n = 17), MI+TVP1022 (IV-only) (n = 8), and Sham (n = 8). $^{*}P < 0.05$ versus MI+Vehicle, $^{\#}P < 0.05$ versus Sham, $^{\$}P < 0.05$ versus IV-only, $^{\varepsilon}P < 0.05$ versus baseline.

blue residues. Collectively, these findings indicate that TVP1022 provided prominent cardioprotection by attenuating post-MI cardiac dysfunction. The analysis shows that the global CS in the vehicle group was reduced at both the AP and the PM levels (by 44% and 41%, respectively) ($P < 0.05$ vs. sham). In the MI+TVP1022 "IV-only" group PM level global CS was reduced by 29%, ($P < 0.05$) (Fig. 3B, C). However, chronic TVP1022 treatment (20 or 40 mg/kg) preserved global CS both at the AP and PM levels ($P < 0.05$ vs. MI+Vehicle, Fig. 3B). Collectively, the echocardiographic measurements further support the cardioprotective efficacy of TVP1022, and emphasis its dose–response effect on attenuation of LV dimensional and functional changes, 14 days post-MI.

Cardiovascular hemodynamic measurements

On day 14, LV performance was evaluated using the Millar P-V conductance catheter system to obtain LV pressure-volume relationships (P-V loops). During the procedure 13 animals died before valuable samples could be obtained by the Millar catheter. Figure 4A depicts typical representative P-V loops obtained from sham, MI+Vehicle, and MI+TVP1022 (40 mg/kg) rats. Compared to the sham group, in the MI+Vehicle group the P-V loops are smaller, the end diastolic volume (EDV) is higher and the P-V loops are shifted to the right, representing cardiac pathophysiological and structural changes corresponding to post-MI remodeling. Hence, the dilated LV (e.g., increased EDV and ESV) and the smaller P-V loop (e.g., low SV, SW, and systolic pressure) characterize

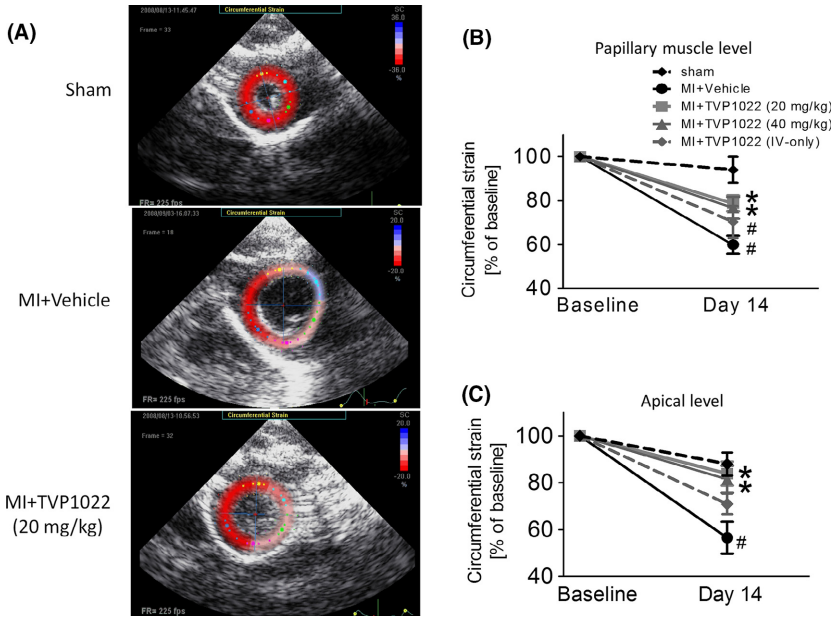

Figure 3. TVP1022 preserved LV global CS 14 days post-MI. (A) Representative CS distribution along the cardiac wall measured at the apical level, obtained from the sham, MI+Vehicle and MI+TVP1022 (20 mg/kg) groups (additional groups are depicted in Fig. S2C). Dark red colors represent strong CS, whereas dark blue colors represent severe stretching; Echocardiographic CS measured at the PM (B) and apical (C) levels 14 days post-MI from the MI+Vehicle (n = 11), MI+TVP1022 (20 mg/kg) (n = 12), MI+TVP1022, (40 mg/kg) (n = 11), MI+TVP1022 (IV-only) (n = 8), and Sham (n = 8) groups. $^{*}P < 0.05$ versus MI+Vehicle, $^{\#}P < 0.05$ versus Sham.

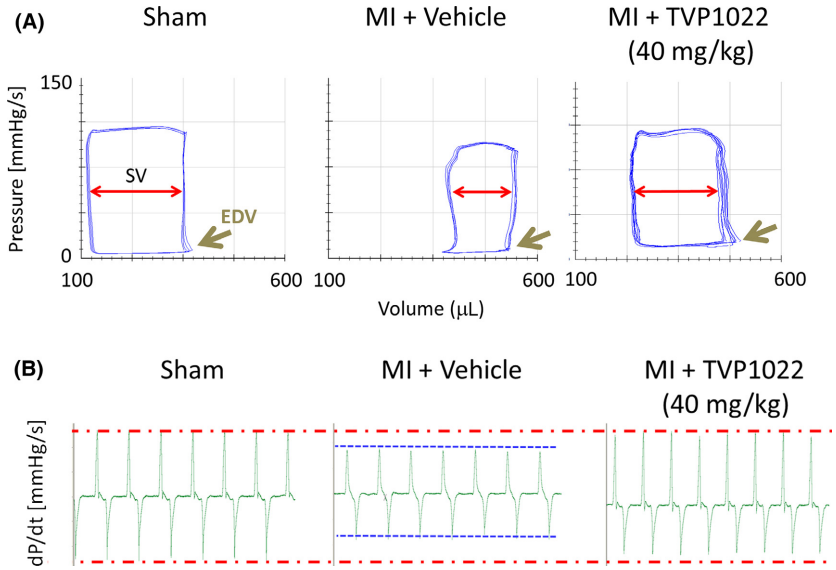

Figure 4. TVP1022 preserved hemodynamics and LV function 14 days post-MI. (A) Representative P-V loops obtained from sham, MI+Vehicle and MI+TVP1022 (40 mg/kg) rats (additional groups are depicted in Fig. S3A). Red arrows – SV, brown arrows – EDV. (B) Representatives dP/dt recordings obtained from the sham, vehicle and TVP1022 (40 mg/kg) treated rats (additional groups are depicted in Fig. S3B). Red lines – Sham max and min dP/dt values, blue lines – MI+Vehicle max and min values.

weaker cardiac muscle. Importantly, these adverse changes were prevented by TVP1022, and thus the dimensions and the position of the loops recorded in TVP1022-treated rats are similar to those of sham rats (Fig. 4A). Furthermore, as seen in Fig. 4B (depicting dP/dt recordings), the reductions (compared to sham) of the dP/dt_{max} and dP/dt_{min} values in the MI+Vehicle group were prevented by the TVP1022 treatment. Table 3 summarizes the LV hemodynamic measurements 14 days post-MI in the different groups. The pressure measurements show no difference in LV end diastolic pressure (LVEDP) between the treatment groups. LV end systolic pressure (LVESP) was comparable between the vehicle, TVP1022-treated rats, and sham (group 5) rats ($P > 0.05$). LVESP was reduced in the vehicle-treated rats compared to the 40 mg/kg TVP1022-treated rats ($P < 0.05$). The maximal systolic LV pressure (LVP max) was lower in the vehicle-treated rats ($P < 0.05$ vs. sham), whereas in the TVP1022-treated rats the pressure was preserved ($P > 0.05$ vs. sham). Impairment of systolic performance after MI was demonstrated by significant reductions in dP/dt_{max} in the vehicle and the TVP1022 (20 mg/kg and IV-only) treated rats ($P < 0.05$ vs. sham). In the TVP1022 (40 mg/kg) group dP/dt_{max} ($P < 0.05$ vs. MI+Vehicle) was preserved and the TVP1022 IV-only treatment attenuated the decrease in dP/dt_{max} ($P < 0.05$ vs. MI+Vehicle). While the maximal rate of pressure relaxation (dP/dt_{min}) was smaller in all MI rats, this decrease was attenuated in the TVP1022 (40 mg/kg and IV-only) groups (Table 3, and Fig. 4B). Additional analysis of the hemodynamic data showed that (Fig. 5): (1) Heart rate was similar in all groups. (2) SV, CO, EF, and SW were reduced in vehicle-treated rats. (3)

Table 3. LV pressure measurements 14 days post-MI. Pressures were measured using the Millar Mikro-Tip® catheter.

Treatment	LVEDP [mmHg]	LVESP [mmHg]	LVP_{max} [mmHg]	dP/dt max [mmHg/sec]	dP/dt min [mmHg/sec]
MI + Vehicle (n = 22)	11.3 ± 1.1	82.8 ± 3.2	#92.5 ± 2.4	#4673 ± 255	#−3580 ± 206
MI+TVP1022 (20 mg/kg) (n = 8)	10 ± 0.2	90.5 ± 8.3	105.2 ± 6.1	#5739 ± 439	#−4502 ± 451
MI+TVP1022 (40 mg/kg) (n = 14)	7.6 ± 0.6	*98.2 ± 2.6	*106.5 ± 2.1	*6944 ± 288	#*−5035 ± 292
MI+TVP1022 IV-only (n = 8) (40 mg/kg)	8.3 ± 0.4	81 ± 3.7	98.8 ± 3.1	#*6322 ± 314	#*−5009 ± 264
Sham (n = 6)	7.8 ± 1	94 ± 4.4	109.8 ± 3.8	8215 ± 496	−7215 ± 455

LVEDP, Left ventricular end diastolic pressure; LVESP, left ventricular end systolic pressure; LVP_{max}, maximum left ventricular pressure; dP/dt_{max}, the maximal peak rate of pressure development; dP/dt_{min}, the maximal rate of pressure decay.
#$P < 0.05$ versus sham.
*$P < 0.05$ versus MI+Vehicle.

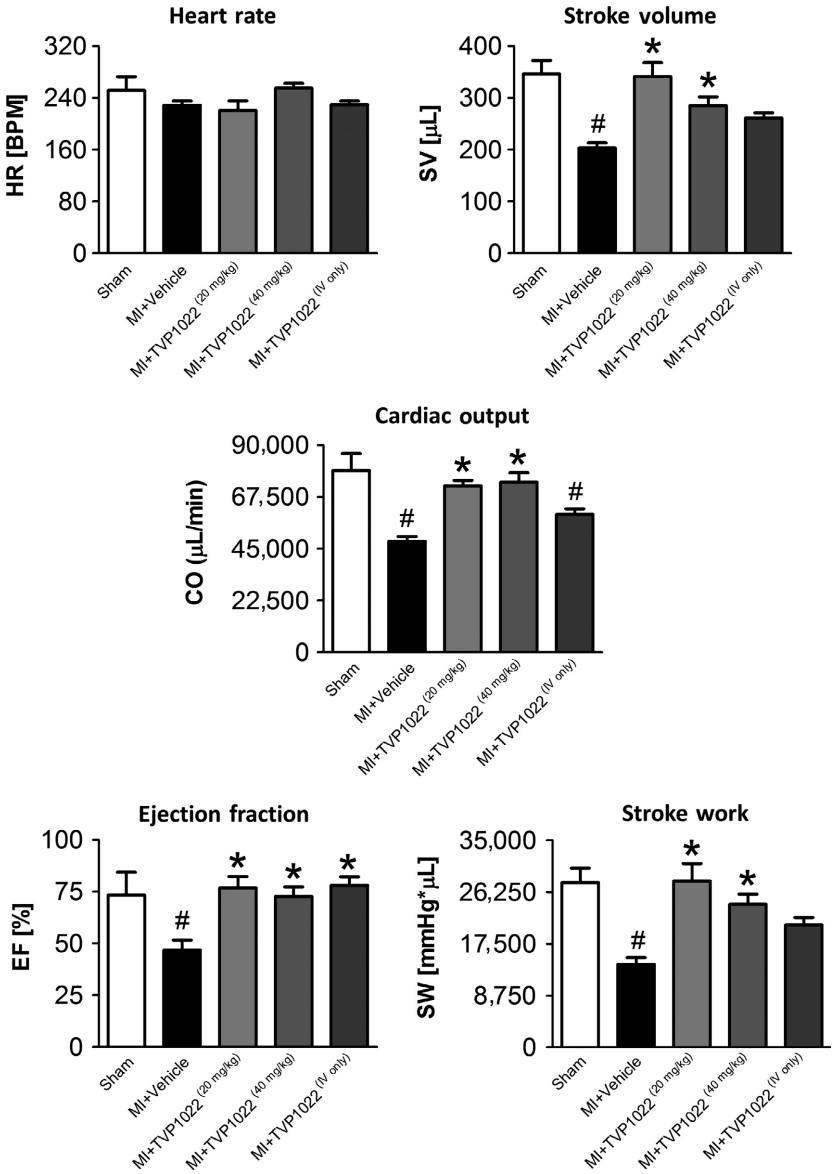

Figure 5. Selected cardiac functional measurements obtained from the different groups: MI+Vehicle (n = 22), MI+TVP1022 (20 mg/kg) (n = 8), MI+TVP1022, (40 mg/kg) (n = 14), MI+TVP1022 (IV-only) (n = 8) and sham (n = 6). $^{*}P < 0.05$ versus MI+Vehicle, $^{\#}P < 0.05$ versus sham.

While chronic TVP1022 treatments preserved these hemodynamic parameters, only EF was preserved in the IV-only group. Collectively, the hemodynamic measurements indicate that TVP1022 attenuated LV dimensional and functional changes 14 days post-MI, thus decreasing the remodeling magnitude.

Fibrosis analysis

Fibrosis represented by collagen volume fraction (CVF), was evaluated by calculating the interstitial collagen in the remote noninfarcted area. Specifically, for the CVF calculation we measured the positive collagen staining (light blue) in Masson's trichrome-stained slides (the viable myocardium stained in bright red). To this end Figure 6A depicts representative Masson's trichrome-stained slides at ×400 magnification from sham, vehicle, and 20 mg/kg TVP1022-treated rats. In agreement with its cardioprotective efficacy, TVP1022 decreased the remote zone interstitial collagen. Accordingly, CVF was lower in the TVP1022 (20 and 40 mg/kg) groups than in the vehicle group ($3.9 \pm 0.5\%$ and $2.9 \pm 0.4\%$ vs. $8.3\% \pm 1.2$, respectively, $P < 0.05$ vs. sham for both) (Fig. 6B), indicating that TVP1022 attenuates ventricular

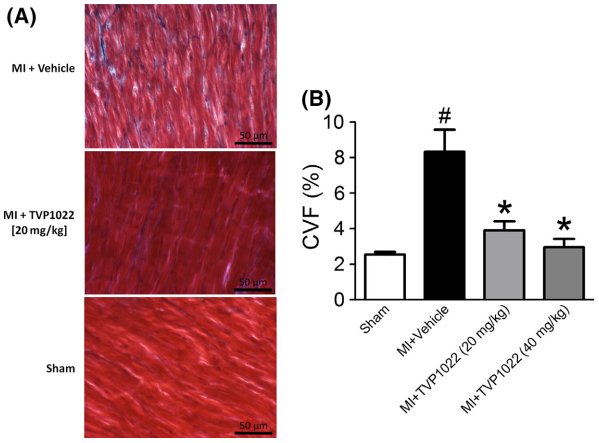

Figure 6. TVP1022 attenuated post-MI myocardial interstitial fibrosis. (A) Representative sections of the myocardium from the remote viable zone of the different treated rats, stained with Masson's trichrome staining at ×400 magnification. Viable myocardium is stained bright red. Fibrosis is stained bright blue. (B) CVF measurements in the treatment groups: MI+Vehicle ($n = 6$), MI+TVP1022 (20 mg/kg) ($n = 6$), MI+TVP1022, (40 mg/kg) ($n = 6$) and sham ($n = 6$). $^{*}P < 0.05$ versus MI+Vehicle, $^{\#}P < 0.05$ versus sham.

fibrosis 14 days post-MI, which is of a major beneficial significance.

TVP1022 attenuated post-MI ventricular hypertrophy

Ventricular hypertrophy was evaluated by measuring diameter and area of cardiomyocytes from the remote tissue and the scar border zone by means of dystrophin staining. To ensure proper sampling only myocytes with a nucleus (stained with DAPI) were measured. As illustrated by the representative sections of scar border tissue, post-MI remodeling was associated with marked hypertrophy (compared to sham), which was partially alleviated in the TVP1022 rat (Fig. 7A). In summary (Fig. 7B–E), post-MI remodeling was associated with marked increase in myocyte area and diameter in the remote tissue and scar zone ($P < 0.05$ vs. sham) (Fig. 7B–E). Overall, TVP1022 administration reduced hypertrophy at both areas. Specifically, TVP1022 attenuated myocyte hypertrophy as indicated by a reduction in myocyte area and diameter ($P < 0.05$ vs. Vehicle) (Fig. 7D, E). At the remote tissue, the vehicle and MI+TVP1022 (IV-only) treated rats were associated with marked increase in myocyte area and diameter compared to the sham rats ($P < 0.05$). Chronic TVP1022 administration prevented myocyte hypertrophy as indicated by the preservation of myocyte area and diameter of the TVP1022 40 mg/kg treated rats compared to the sham rats ($P > 0.05$ vs. sham, or vehicle) (Fig. 7B, C). In summary, TVP1022 treatment attenuated and even prevented post-MI hypertrophy not only at the whole organ level (i.e., the heart) but at the cellular level as well.

One of the key indices of progressive ventricular dilatation and development of CHF is increased BNP level (Ohata et al. 2004). Accordingly, LV BNP levels were determined by immunofluorescence staining for BNP (Fig. 8). Figure 8A illustrates representative myocardial sections obtained from sham, vehicle, and 40 mg/kg TVP1022-treated rats stained for BNP (red) and nuclei with (DAPI, blue). This figure shows that: (1) BNP mainly localized in cardiomyocytes in the nuclear/perinuclear area; (2) BNP was more abundant in the MI+Vehicle rat than in the sham rat; (3) BNP expression was markedly lower in the TVP1022 (40 mg/kg) rat compared to the MI+Vehicle rat. In agreement with its potent cardioprotective efficacy chronic TVP1022 treatment markedly attenuated ($P < 0.05$ vs. vehicle) post-MI increase in tissue BNP levels, a key hallmark of CHF (Fig. 8B).

Discussion

Based on our previous findings demonstrating the cardioprotective efficacy of TVP1022 in a variety of cardiac pathologies (Kleiner et al. 2008; Berdichevski et al. 2010; Abassi et al. 2011; Ertracht et al. 2011; Malka et al. 2015), in this study we tested the hypothesis that TVP1022 will provide cardioprotection against I/R injury and post-MI left ventricle (LV) remodeling in rats. To this end, we employed a rat I/R model replicating the clinical scenario of acute MI patients with a cardioprotective drug administered prior to and following reperfusion therapy and at a follow-up period which mimics post-MI healing, repair, and remodeling phases. Our key findings demonstrate that a combination of pre and postreperfusion administration of TVP1022: (1) markedly attenuated post-MI remodeling at the organ, tissue, and the cellular levels; (2) preserved cardiac function 14 days post-MI; (3) Acute treatment (day of the MI) with TVP1022 is sufficient for achieving cardioprotection by decreasing scar size; However, there are substantial benefits from the chronic TVP1022 administration.

For evaluating post-MI remodeling, we determined cardiac functional changes by echocardiographic and direct hemodynamic measurements, and cardiac markers and structural changes by histopathological analysis. The I/R rats displayed cardiac dysfunction along with profound cardiac remodeling characterized by increased LV dimensions, increased tissue fibrosis and elevated heart and myocyte size. Direct measurements of cardiac performance using the Millar P-V conductance catheter system demonstrated deformed P-V loops in the I/R rats; the reductions in SV, SW, systolic pressure, CO, dP/dt_{max},

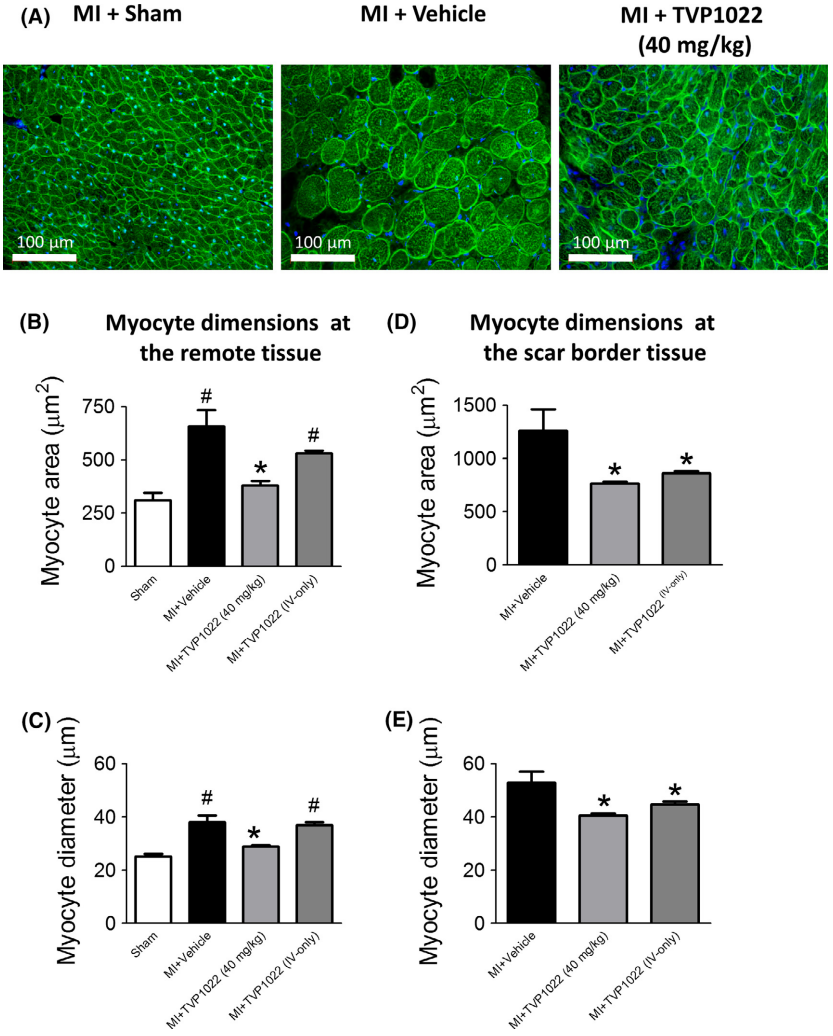

Figure 7. TVP1022 attenuated post-MI myocyte hypertrophy. Representative sections of the myocardium from the scar border tissue of the different treated rats, stained for dystrophin (green), and for nuclei with DAPI (blue), at ×200 magnification (A) (additional group is depicted in Fig. S4A). Myocyte dimensions: at the remote tissue – area (B), diameter (C); at the scar border tissue – area (D), diameter (E) of the treatment groups: MI+Vehicle (n = 5), MI+TVP1022 (40 mg/kg) (n = 5), MI+TVP1022 (IV-only) (n = 4), and sham (n = 4). *P < 0.05 versus MI+Vehicle, $^{\#}P$ < 0.05 versus sham, ^{ǂ}P < 0.05 versus MI+TVP1022 (IV-only).

and dP/dt_{min} are all indicative of reduced cardiac performance and weakened cardiac muscle. Furthermore, the increased LVEDV and LVESV indicate ventricular dilation. These findings are comparable to the results of other post-MI remodeling studies (Lei et al. 2013; Berthiaume et al. 2014; Kim et al. 2014). In addition to the direct hemodynamic measurements, cardiac function was also evaluated by echocardiography. The I/R rats displayed marked decrease in FS, EF, and CS. While FS and EF are well accepted measures of cardiac function, CS is a rather new measurement considered to be more accurate (Rappaport et al. 2006; Popović et al. 2007; Malka et al. 2015). FS and EF adequately describe cardiac function in the absence of regional wall-motion abnormalities; however, the small size of the rat heart and its high beating rate preclude their accurate estimation in case of regional wall-motion abnormalities (Liao et al. 2012). CS is considered to be a sensitive measurement as it can be measured at two distinct levels (PM and AP) using multiple points on the cardiac wall circumference (Rappaport et al. 2006), thus improving its resolution post-MI.

Post-MI ventricular remodeling is directly associated with the progression to heart failure and increased morbidity and mortality (Sutton and Sharpe 2000). Because ventricular remodeling is a continuous process contributing to functional deterioration long after the primary ischemic insult, it presents a therapeutic target for chronically delivered cardioprotective drugs. In accordance with

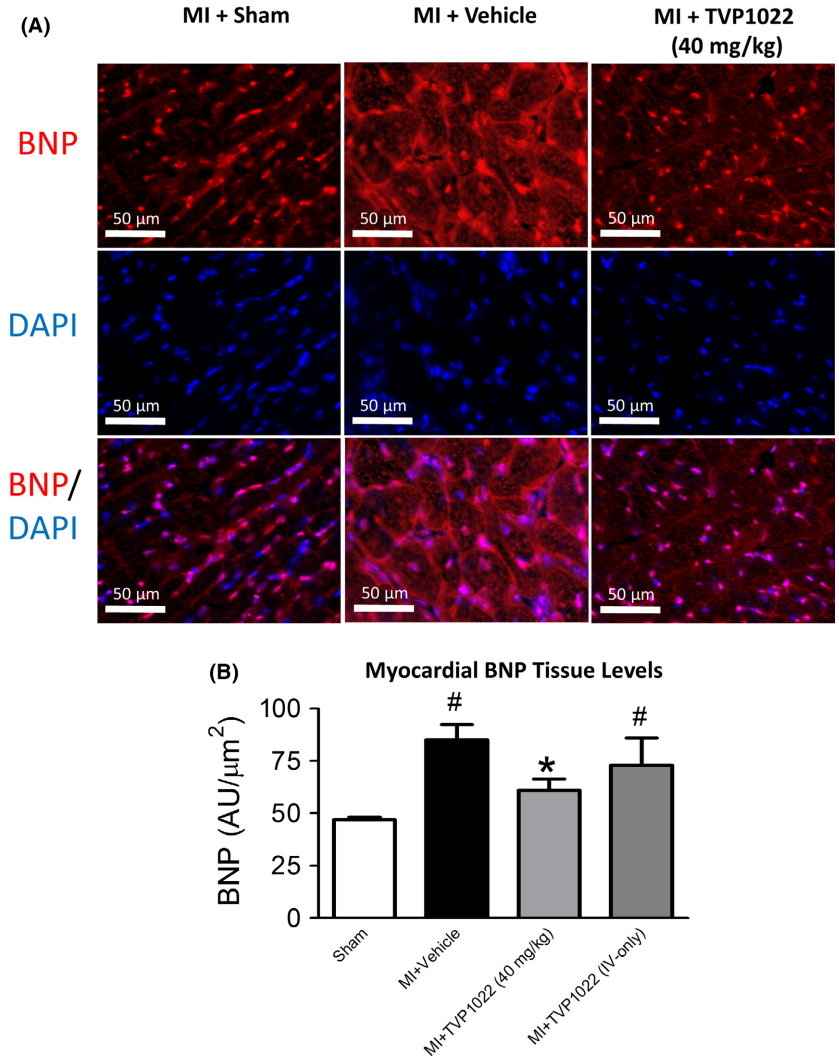

Figure 8. TVP1022 attenuated post-MI myocardial BNP levels. (A) Representative sections of the myocardium obtained from the different treatment groups, stained for BNP (red), and for nuclei with DAPI (blue), at ×400 magnifications (additional groups are depicted in Fig. S4B). (B) Myocardial BNP levels of the treatment groups: MI+Vehicle (n = 5), MI+TVP1022 (40 mg/kg) (n = 5), MI+TVP1022 (IV-only) (n = 4), and sham (n = 4). $^{*}P < 0.05$ versus MI+Vehicle, $^{\#}P < 0.05$ versus sham.

our previous in vivo studies, TVP1022 markedly attenuated I/R injury and post-MI remodeling (Abassi et al. 2011; Ertracht et al. 2011; Malka et al. 2015).

Accordingly, we evaluated LV dilation by echocardiographic measures LVESA and LVEDA, cardiac hypertrophy by calculating HW to BW ratio and cellular hypertrophy by dystrophin and collagen stainings. TVP1022 treatment markedly attenuated LV dilation, organ, and cellular hypertrophy. Furthermore, we evaluated interstitial fibrosis in the remote noninfarcted myocardium, and found that TVP1022 pronouncedly reduced interstitial fibrosis. The cardiac remodeling process is characterized by alternations in tissue structure, particularly fibrous tissue formation in the infarcted and noninfarcted myocardium (Volders et al. 1993; Beltrami et al. 1994; Malka et al. 2015). Fibrosis in the remote noninfarcted tissue is considered as the main cause for post-MI ventricular remodeling (Volders et al. 1993; Beltrami et al. 1994; Malka et al. 2015). The fibrous tissue response of the cardiac interstitium is thought to be responsible for abnormal ventricular stiffness and has also been suggested to account for a spectrum of ventricular dysfunction that involve either the systolic or diastolic phases of the cardiac cycle or both (Weber and Brilla 1991; Malka et al. 2015). Furthermore, Sabbah et al. found decreased capillary density and increased oxygen diffusion distance in viable LV regions that manifest severe interstitial fibrosis suggesting that this phenomenon

may be associated with localized chronic hypoxia; a condition which is likely to adversely influence the functional capacity and ultimately the viability of the collagen encircled cardiomyocytes (Sabbah et al. 1993). In agreement with our previous studies demonstrating that TVP1022 attenuated LV remodeling in volume-overload CHF rats and in pigs post I/R injury (Abassi et al. 2011; Malka et al. 2015), TVP1022 administration markedly reduced the interstitial fibrosis 14 days post-MI.

Functionally, we found that TVP1022 treatment attenuated the decline and even preserved cardiac function. Specifically, the echocardiographic measures FS, EF, and CS, and most of the direct hemodynamic indexes such as SV, SW, CO, dP/dt_{max}, and dP/dt_{min} were markedly improved by the TVP1022 treatments.

BNP plays a compensatory role in cardiac disease states due to its diuretic, natriuretic, vasodilating actions and inhibitory effects on the RAAS and endothelin systems (Mair 2008). Furthermore, BNP rather than atrial natureticpeptide (ANP) correlates better with the severity of CHF (Nishikimi et al. 2006). Therefore, plasma BNP has been suggested (and lately used) to diagnose heart failure (Abassi et al. 2004). In this study, tissue BNP levels were dramatically reduced following the chronic treatment of TVP1022. BNP is mainly produced by over-stretched ventricular myocytes (Ogawa et al. 1991). Thus, in the current setup reduced BNP levels can result from direct effect of TVP1022 on the myocytes, or attenuation of myocytes stretch due to the overall improved cardiac structure and function. Further investigation is needed in order to decipher the effect of TVP1022 on BNP levels.

In conclusion, TVP1022 treatment showed beneficial effects as it attenuated cardiac dysfunction and the remodeling processes post-MI, indicating that TVP1022 should be considered as a novel drug for treating MI injury and cardiac remodeling. If the equivalent findings can be translated to the clinical arena, the beneficial impact on postinfarction heart failure development with its associated morbidity and mortality is expected to be profound.

Acknowledgments

TVP1022 was kindly donated by TEVA (Netanya, Israel).

Author Contribution

Malka, Ertracht, Bachner-Hinenzon, Reiter, and Binah participated in research design. Malka, Ertracht, and Reiter conducted the experiments. Malka and Bachner-Hinenzon performed data analysis. Malka, Ertracht, and Binah wrote or contributed to the writing of the manuscript.

Disclosure

None declared.

References

Abassi Z, Karram T, Ellaham S, Winaver J, Hoffman A (2004). Implications of the natriuretic peptide system in the pathogenesis of heart failure: diagnostic and therapeutic importance. Pharmacol Ther 102: 223–241.

Abassi ZA, Barac YD, Kostin S, Roguin A, Ovcharenko E, Awad H, et al. (2011). TVP1022 attenuates cardiac remodeling and kidney dysfunction in experimental volume overload-induced congestive heart failure. Circ Heart Fail 4: 463–473.

Antman EM, Hand M, Armstrong PW, Bates ER, Green LA, Halasyamani LK, et al. (2008). 2007 focused update of the ACC/AHA 2004 guidelines for the management of patients with ST-elevation myocardial infarction: a report of the American College of Cardiology/American Heart Association Task Force on Practice Guidelines. J Am Coll Cardiol 51: 210–247.

Arias T, Chen J, Fayad ZA, Fuster V, Hajjar RJ, Chemaly ER (2013). Comparison of echocardiographic measurements of left ventricular volumes to full volume magnetic resonance imaging in normal and diseased rats. J Am Soc Echocardiogr 26: 910–918.

Beltrami CA, Finato N, Rocco M, Feruglio GA, Puricelli C, Cigola E, et al. (1994). Structural basis of end-stage failure in ischemic cardiomyopathy in humans. Circulation 89: 151–163.

Berdichevski A, Meiry G, Milman F, Reiter I, Sedan O, Eliyahu S, et al. (2010). Tvp 1022 protects neonatal rat ventricular myocytes against doxorubicin-induced functional derangements. J Pharmacol Exp Ther 332: 413–420.

Berthiaume JM, Azam SM, Hoit BD, Chandler MP (2014). Cardioprotective effects of dietary lipids evident in the time-dependent alterations of cardiac function and gene expression following myocardial infarction. Physiol Rep 2: 1–14.

Bhindi R, Witting PK, McMahon AC, Khachigian LM, Lowe HC (2006). Rat models of myocardial infarction. Pathogenetic insights and clinical relevance. Thromb Haemost 96: 602–610.

Black SC (2000). In vivo models of myocardial ischemia and reperfusion injury: Application to drug discovery and evaluation. J Pharmacol Toxicol Methods 43: 153–167.

Dorn GW II (2009). Apoptotic and non-apoptotic programmed cardiomyocyte death in ventricular remodelling. Cardiovasc Res 81: 465–473.

Ertracht O, Liani E, Bachner-Hinenzon N, Bar-Am O, Frolov L, Ovcharenko E, et al. (2011). The cardioprotective efficacy of tvp1022 in a rat model of ischaemia/reperfusion. Br J Pharmacol 163: 755–769.

Huang W, Chen Y, Shohami E, Weinstock M (1999). Neuroprotective effect of rasagiline, a selective monoamine

oxidase-b inhibitor, against closed head injury in the mouse. Eur J Pharmacol 366: 127–135.

Jalil JE, Doering CW, Janicki JS, Pick R, Shroff SG, Weber KT (1989). Fibrillar collagen and myocardial stiffness in the intact hypertrophied rat left ventricle. Circ Res 64: 1041–1050.

Kim YS, Kang WS, Kwon JS, Hong MH, Jeong H-Y, Jeong HC, et al. (2014). Protective role of 5-azacytidine on myocardial infarction is associated with modulation of macrophage phenotype and inhibition of fibrosis. J Cell Mol Med 18: 1018–1027.

Kleiner Y, Bar-Am O, Amit T, Berdichevski A, Liani E, Maor G, et al. (2008). Tvp 1022 and propargylamine protect neonatal rat ventricular myocytes against doxorubicin-induced and serum starvation-induced cardiotoxicity. J Cardiovasc Pharmacol 52: 268–277.

Lei J, Xue S, Wu W, Zhou S, Zhang Y, Yuan G, et al. (2013). Sdc1 overexpression inhibits the p38 MAPK pathway and lessens fibrotic ventricular remodeling in MI rats. Inflammation 36: 603–615.

Liao S, Ruan Q, Lin M, Yan L (2012). Value of segmental myocardial strain by 2-dimensional strain echocardiography for assessment of scar area induced in a rat model of myocardial infarction. Cardiovasc. Ultrasound 10: 17.

Mair J (2008). Biochemistry of B-type natriuretic peptide–where are we now? Clin Chem Lab Med 46: 1507–1514.

Malka A, Meerkin D, Barac YD, Malits E, Bachner-Hinenzon N, Carasso S, et al. (2015). TVP1022: a Novel Cardioprotective Drug Attenuates Left Ventricular Remodeling After Ischemia/Reperfusion in Pigs. J Cardiovasc Pharmacol 66: 214–222.

Nishikimi T, Maeda N, Matsuoka H (2006). The role of natriuretic peptides in cardioprotection. Cardiovasc Res 69: 318–328.

Ogawa Y, Nakao K, Mukoyama M, Hosoda K, Shirakami G, Arai H, et al. (1991). Natriuretic peptides as cardiac hormones in normotensive and spontaneously hypertensive rats. The ventricle is a major site of synthesis and secretion of brain natriuretic peptide. Circ Res 69: 491–500.

Ohata T, Sakakibara T, Takano H, Izutani H (2004). Plasma brain natriuretic peptide reflects left ventricular function during percutaneous cardiopulmonary support. Ann Thorac Surg 77: 164–167.

Pacher P, Nagayama T, Mukhopadhyay P, Bátkai S, Kass DA (2008). Measurement of cardiac function using pressure-volume conductance catheter technique in mice and rats. Nat Protoc 3: 1422–1434.

Popović ZB, Benejam C, Bian J, Mal N, Drinko J, Lee K, et al. (2007). Speckle-tracking echocardiography correctly identifies segmental left ventricular dysfunction induced by scarring in a rat model of myocardial infarction. Am J Physiol Heart Circ Physiol 292: 2809–2816.

Rappaport D, Adam D, Lysyansky P, Riesner S (2006). Assessment of myocardial regional strain and strain rate by tissue tracking in B-mode echocardiograms. Ultrasound Med Biol 32: 1181–1192.

Sabbah HN, Hansen-Smith F, Sharov VG, Kono T, Lesch M, Gengo PJ, et al. (1993). Decreased proportion of type I myofibers in skeletal muscle of dogs with chronic heart failure. Circulation 87: 1729–1737.

Spinale FG (2010). Amplified bioactive signaling and proteolytic enzymes following ischemia reperfusion and aging: remodeling pathways that are not like a fine wine. Circulation 122: 322–324.

Sutton MG, Sharpe N (2000). Left ventricular remodeling after myocardial infarction: pathophysiology and therapy. Circulation 101: 2981–2988.

Volders PG, Willems IE, Cleutjens JP, Arends JW, Havenith MG, Daemen MJ (1993). Interstitial collagen is increased in the non-infarcted human myocardium after myocardial infarction. J Mol Cell Cardiol 25: 1317–1323.

Weber KT, Brilla CG (1991). Pathological hypertrophy and cardiac interstitium. Fibrosis and renin-angiotensin-aldosterone system. Circulation 83: 1849–1865.

Yellon DM, Hausenloy DJ (2007). Myocardial reperfusion injury. N Engl J Med 357: 1121–1135.

Youdim MB, Bar Am O, Yogev-Falach M, Weinreb O, Maruyama W, Naoi M, et al. (2005). Rasagiline: neurodegeneration, neuroprotection, and mitochondrial permeability transition. J Neurosci Res 79: 172–179.

Supporting Information

Additional Supporting Information may be found online in the supporting information tab for this article:

Figure S1. The chemical structure of TVP1022 (*N*-propargyl-1-(*S*)-aminoindan).

Figure S2. (A) Representative apical level echocardiographic two-dimensional (2D) mode end-diastolic cines of the TVP1022 20 mg/kg and TVP1022 (IV-only) groups 14 days post-MI, white tracing – LV cavity. (B) Representative echocardiographic M-mode cines obtained at the PM level for the TVP1022 40 mg/kg and TVP1022 (IV-Only) groups. (C) Representative CS distribution along the cardiac wall measured at the apical level, obtained from the TVP1022 40 mg/kg and TVP1022 (IV-only) groups. Dark red colors represent strong CS, whereas dark blue colors represent severe stretching.

Figure S3. (A) Representative P-V loops obtained from TVP1022 20 mg/kg and TVP1022 (IV-only) rats. Red arrows – SV, brown arrows – EDV. (B) Representatives dP/dt recordings obtained from TVP1022 20 mg/kg and

TVP1022 (IV-only) rats. Red lines – Sham max and min dP/dt values.

Figure S4. (A) Representative sections of the myocardium from the remote viable zone of the TVP1022 40 mg/kg treated rats, stained with Masson's trichrome staining at ×400 magnification. Viable myocardium is stained bright red. Fibrosis is stained bright blue. (B) Representative sections of the myocardium from the scar border tissue of a TVP1022 (IV-only) treated rat, stained for dystrophin (green), and for nuclei with DAPI (blue), at ×200 magnification. (C) Representative sections of the myocardium obtained from a TVP1022 (IV-only) treated rat groups, stained for BNP (red), and for nuclei with DAPI (blue), at ×400 magnifications.